Ferromagnetic - paramagnetic phase diagram of the Kondo lattice

1996 J. Phys.: Condens. Matter 8 7941

(http://iopscience.iop.org/0953-8984/8/42/013)

J. Phys.: Condens. Matter **8** (1996) 7941–7956. Printed in the UK

Ferromagnetic–paramagnetic phase diagram of the Kondo lattice

Zheng-zhong Li, Ming Zhuang and Ming-wen Xiao
Department of Physics, Nanjing University, Nanjing, 210093, People's Republic of China

Received 9 May 1996, in final form 2 July 1996

Abstract. A theory which can easily be used to discuss the competition between ferromagnetic order and the Kondo effect is presented in this paper. The magnetic order parameters of conduction and localized electrons as well as the hybridization term describing the Kondo effect are introduced simultaneously in a Kondo lattice model using the functional integral method. At zero temperature, quite a complete phase diagram of ferromagnetic and paramagnetic (Kondo) states is obtained in the static saddle-point approximation. At finite temperatures, the dependences of the Curie temperature T_C and the total magnetization m_t on the exchange-coupling strength $|J|$ for various concentrations n_c of conduction electrons, are also given by the theory. The main results are in qualitative agreement with experimental observations in heavy-fermion ferromagnets.

1. Introduction

It is generally agreed that the heavy-fermion (HF) systems can be classified into four broad groups according to their ground-state properties: superconducting, insulating, magnetically ordered or enhanced Pauli paramagnetic. The duality between the latter two cases is concerned with the weak stability of paramagnetic HF metals against HF magnets. As to the HF materials with magnetically ordered ground states, early experimental observations indicated that HF magnets usually exhibit some antiferromagnetic type of order [1]. However, there is no *a priori* reason to exclude ferromagnetism in HF systems, and a series of HF ferromagnets have recently been discovered, e.g. $CeSi_x$ ($x < 1.85$) [2], $CeNi_xPt_{1-x}$ ($x < 0.9$) [3], CePdSb [4] and $CeRh_3B_2$ [5]. These Ce compounds constitute a ferromagnetic Kondo-lattice (FMKL) system in which the RKKY exchange interaction competes with the Kondo effect; their low-temperature properties upon doping or under applied pressure (i.e. the variations in T_C and m_t with changing $|J|$ or n_c) attract great interest but are not well understood so far [5]. This is still an active field in current research on the HF systems.

Theoretically, the Kondo lattice model (KLM) is a generalization of the single-ion Kondo system to the concentrated case of a lattice with one Kondo ion at each lattice site. Doniach [6] first examined a 'Kondo necklace' (one-dimensional Kondo lattice (KL)) problem in the mean-field approximation (MFA) and concluded that at $T = 0$ a second-order phase transition separates the antiferromagnetic ground state from the non-magnetic (Kondo) state at a critical value of $|J| = |J_c|$, and that for $|J| < |J_c|$ the ground state consists of antiferromagnetic ordered but partially compensated f spins. On the basis of this result, he proposed a schematic phase diagram in the T–$|J|$ plane where the magnetic-ordering temperature as a function of $|J|$ resembles a bell-shaped curve [7]. The subsequent study on

0953-8984/96/427941+16$19.50

a three-dimensional (3D) KL given by Lacroix and Cyrot [8] indicated that antiferromagnetic and ferromagnetic ground states are both possible, depending on the extent of band filling, i.e. on the number n_c of conduction electrons per site. Fazekas and Müller-Hartmann [9] used a variational method to investigate the phase diagram of the FMKL for arbitrary $|J|$ and n_c. At zero temperature, they obtained phase boundaries between non-magnetic (Kondo) and different magnetic states including saturated and RKKY ferromagnetic states (RFSs); they are similar to those given by Lacroix and Cyrot [8] in the whole n_c–$|J|$ plane. The only difference is that in [9] the ferromagnetic–Kondo phase boundary has been pushed down to lower but more reasonable values of $|J|$ than in [8] owing to the lattice enhancement of the Kondo effect. However, a coexistent phase where magnetic order and the Kondo effect are present simultaneously was neglected in both [8] and [9]; it might be a stable phase between pure Kondo and pure magnetic phases. Following closely the work of Lacroix and Cyrot [8], Li and Qiu [10] have included the coexistent phase in the n_c–$|J|$ plane at $T = 0$ by taking into account the competition between the Kondo effect and ferromagnetic order. In [10], two new phase boundaries, including the boundaries between the coexistent phase and the Kondo phase or saturated ferromagnetic phase, have been obtained, but we failed to get the boundary between the coexistent phase and RKKY ferromagnetic phase because the Fermi level was inattentively restricted only in the lower hybridization bands for both up and down spins. In fact, the Fermi level of the coexistent phase can shift consecutively from the lower band through the gap to the upper band of up (or down) spin with increase in n_c at a definite value of $|J|$ or by changing $|J|$ at a definite n_c [11, 12]. Therefore, a systematic study on the magnetic–non-magnetic phase boundaries of the FMKL in the n_c–$|J|$ plane at $T = 0$ and the extension to $T > 0$ so as to obtain a microscopic derivation of T_c–$|J|$ curves for various n_c is still needed.

In this paper, we attempt to investigate the paramagnetic–ferromagnetic phase diagram of a FMKL by adopting the functional integral formalism with four auxiliary Bose fields in analogy to [13, 14], which can provide a simple description of the competition between magnetic ordering and the Kondo effect. The rest of the paper is organized as follows. In section 2, we introduce the functional integral formalism of a FMKL and deduce the effective Hamiltonian and its self-consistent mean-field (SCMF) equations in the static saddle-point approximation. In section 3, we present a rather complete ground-state phase diagram (GSPD) in the n_c–$|J|$ plane at $T = 0$ based on comparing the ground-state energies (GSEs) of different phases. It also includes a detailed analysis of the m_t–$|J|$ curves for arbitrary concentration n_c. In section 4, the bell-shaped T_C–$|J|$ curves and their variation with n_c are carried out by solving the SCMF equations at $T > 0$. Finally, we summarize the main conclusions of this paper in section 5, where an attempt to compare our theoretical results with experimental observations in HF ferromagnets is also included.

2. Theoretical model and related formulae of the ferromagnetic Kondo lattice

2.1. Kondo lattice model

In the KLM, there is a one f spin on each site of the lattice; it interacts with conduction electrons through s–f exchange interaction. Usually, a periodic s–f exchange Hamiltonian

$$H = \sum_{\boldsymbol{k}\sigma} \epsilon_{\boldsymbol{k}} c^{\dagger}_{\boldsymbol{k}\sigma} c_{\boldsymbol{k}\sigma} - J \sum_{i\alpha\beta} c^{\dagger}_{i\alpha} c_{i\beta} (\boldsymbol{\sigma}_{\alpha\beta} \cdot \boldsymbol{S}_i) \tag{1}$$

is adopted to describe the KLM. Here, $J(< 0)$ is the strength of s–f exchange coupling, $\boldsymbol{S}_i$ is the f-spin operator of the rare-earth ion on the site i, $\boldsymbol{\sigma}_{\alpha\beta}$ are the elements of Pauli

matrices, $\epsilon_{\boldsymbol{k}}$ is the band energy of conduction electrons, and $c^{\dagger}_{\boldsymbol{k}\sigma}(c^{\dagger}_{i\sigma})$ creates a conduction electron with spin σ and wavevector $\boldsymbol{k}$ (or on the site i).

In the spin-$\frac{1}{2}$ case, one can use the so-called pseudo-fermion representation for the localized f spins:

$$\boldsymbol{S}^{\alpha\beta}_{if} = \tfrac{1}{2}\sum_{\alpha\beta} f^{\dagger}_{i\alpha}\boldsymbol{\sigma}_{\alpha\beta}f_{i\beta} \tag{2}$$

provided that we work in the subspace such that

$$Q_i = \sum_{\sigma} f^{\dagger}_{i\sigma}f_{i\sigma} = 1 \qquad (i = 1, \ldots, N) \tag{3}$$

where N is the number of lattice sites. Physically, constraint (3) denotes that the number of f electrons at each site i is strictly one. In terms of the pseudo-fermion representation (2), we can rewrite the KL Hamiltonian (1) as

$$\begin{aligned} H = \sum_{\boldsymbol{k}\sigma}\epsilon_{\boldsymbol{k}}c^{\dagger}_{\boldsymbol{k}\sigma}c_{\boldsymbol{k}\sigma} &+ \tfrac{1}{2}J\sum_{i}[(c^{\dagger}_{i\uparrow}f_{i\uparrow} + f^{\dagger}_{i\downarrow}c_{i\downarrow})^2 + (c^{\dagger}_{i\downarrow}f_{i\downarrow} + f^{\dagger}_{i\uparrow}c_{i\uparrow})^2] \\ &-\tfrac{1}{8}J\sum_{i}\{[(c^{\dagger}_{i\uparrow}c_{i\uparrow} - c^{\dagger}_{i\downarrow}c_{i\downarrow}) + (f^{\dagger}_{i\uparrow}f_{i\uparrow} - f^{\dagger}_{i\downarrow}f_{i\downarrow})]^2 \\ &-[(c^{\dagger}_{i\uparrow}c_{i\uparrow} - c^{\dagger}_{i\downarrow}c_{i\downarrow}) - (f^{\dagger}_{i\uparrow}f_{i\uparrow} - f^{\dagger}_{i\downarrow}f_{i\downarrow})]^2\} \end{aligned} \tag{4}$$

where $f^{\dagger}_{i\sigma}$ and $f_{i\sigma}$ are the creation and annihilation operators, respectively, in the Wannier representation for the localized f electrons. It is worth noting that in (4) the interaction terms with pre-factor $\frac{1}{2}J$ represent the processes of s–f hybridizations which favour the Kondo effect, and the others, with pre-factor $-\frac{1}{8}J$, are responsible for the magnetizations of conduction and f electrons which describe the magnetic ordering effect. Therefore, the expressions for interaction terms given in (4) are convenient for us to study the competition between the two effects.

The partition function of the KL Hamiltonian (4) subject to the constraint Q_i can, using the technique introduced by Read and Newns [15], be expressed in the form

$$Z = \int_{-i\pi/\beta}^{i\pi/\beta}\prod_{i}\frac{\beta\,\mathrm{d}\lambda_i}{2\pi}\,\mathrm{Tr}(\exp\{-\beta[H(\lambda) - \mu N_t]\}) \tag{5}$$

with

$$H(\lambda) = H + \sum_{i}\lambda_i\left(\sum_{\sigma} f^{\dagger}_{i\sigma}f_{i\sigma} - 1\right) \tag{6a}$$

and

$$N_t = \sum_{\boldsymbol{k}\sigma} c^{\dagger}_{\boldsymbol{k}\sigma}c_{\boldsymbol{k}\sigma} + \sum_{i\sigma} f^{\dagger}_{i\sigma}f_{i\sigma}. \tag{6b}$$

The advantage is that the trace for $H(\lambda)$ can still be calculated in whole Hilbert space, and then the constraint will be imposed by the final integrations over all the λ_i via the standard formula for a Krönecker delta function.

2.2. Functional integral formalism

In the functional integral formalism, the partition function of the KLM is written as

$$Z = \int_{-i\pi/\beta}^{i\pi/\beta}\prod_{i}\frac{\beta\,\mathrm{d}\lambda_i}{2\pi}\int\mathcal{D}\prod_{i\sigma}c^{\dagger}_{i\sigma}c_{i\sigma}f^{\dagger}_{i\sigma}f_{i\sigma}\exp\left(-\int_0^{\beta}\mathrm{d}\tau\,\mathcal{L}(\tau)\right) \tag{7}$$

with

$$\mathcal{L}(\tau) = \sum_{k\sigma} c^{\dagger}_{k\sigma}(\tau)\frac{\mathrm{d}}{\mathrm{d}\tau}c_{k\sigma}(\tau) + \sum_{i\sigma} f^{\dagger}_{i\sigma}(\tau)\frac{\mathrm{d}}{\mathrm{d}\tau}f_{i\sigma}(\tau) + H(\lambda,\tau) - \mu N_t \qquad (8)$$

where $c_{k\sigma}(\tau)$ and $f_{i\sigma}(\tau)$ are anticommutating Grassman variables. Here, $\mathcal{D}\prod_{i\sigma} c_{i\sigma}\ldots$ is the shorthand for $\prod_{i\sigma}\mathrm{d}c^{\dagger}_{i\sigma}(\tau)\ldots$.

The interaction term can be reformulated through introducing auxiliary Bose field with the well known Stratonovich–Hubbard transformation

$$\exp(\alpha A^2) = \left[\frac{\alpha}{\pi}\right]^{1/2}\int_{-\infty}^{+\infty}\mathrm{d}x\,\exp[-(\alpha x^2 + 2\alpha A x)]. \qquad (9)$$

For the interaction terms of $H(\lambda)$ expressed in equations (4)–(6), we can introduce four auxiliary Bose fields: two 'internal magnetic fields' $m_{is}(\tau)$ and $m_{if}(\tau)$, which are responsible for the occurrence of magnetic ordering; a real Bose field $x_i(\tau)$, which describes a fictitious s–f hybridization and gives the Kondo effect [8]; $\lambda_i(\tau)$, which originates from the parameter λ_i of the constraint (3) and becomes an auxiliary Bose field now owing to a gauge transformation given by Read and Newns [15]. The partition function (7) is then written as

$$Z = \int \mathcal{D}\prod_{i\sigma} c^{\dagger}_{i\sigma}c_{i\sigma}f^{\dagger}_{i\sigma}f_{i\sigma}\lambda_i x_i m_{is}m_{if}\exp\left(-\int_0^{\beta}\mathrm{d}\tau\,\mathcal{L}(\tau)\right) \qquad (10)$$

where

$$\mathcal{L}(\tau) = \sum_{k\sigma} c^{\dagger}_{k\sigma}(\tau)\frac{\mathrm{d}}{\mathrm{d}\tau}c_{k\sigma}(\tau) + \sum_{i\sigma} f^{\dagger}_{i\sigma}(\tau)\frac{\mathrm{d}}{\mathrm{d}\tau}f_{i\sigma}(\tau) + H_{eff}(\tau) - \mu N_t \qquad (11)$$

with the imaginary time-dependent effective Hamiltonian

$$\begin{aligned} H_{eff}(\tau) = {} & \sum_{k\sigma}\epsilon_k c^{\dagger}_{k\sigma}c_{k\sigma} + \sum_i \lambda_i(\tau)\left(\sum_{\sigma} f^{\dagger}_{i\sigma}f_{i\sigma} - 1\right) \\ & \times J\sum_{i\sigma} x_i(\tau)(f^{\dagger}_{i\sigma}c_{i\sigma} + c^{\dagger}_{i\sigma}f_{i\sigma}) + \tfrac{1}{2}J\sum_i m_{is}(\tau)\left(\sum_{\sigma}\sigma f^{\dagger}_{i\sigma}f_{i\sigma}\right) \\ & -\tfrac{1}{2}\sum_i m_{if}(\tau)\left(\sum_{\sigma}\sigma c^{\dagger}_{i\sigma}c_{i\sigma}\right) - J\sum_i x_i^2(\tau) - \tfrac{1}{2}J\sum_i m_{is}(\tau)m_{if}(\tau) \end{aligned} \qquad (12)$$

which is similar to that proposed by Lacroix [14]. In the effective Hamiltonian (12), the interaction terms containing four fermion operators in (4) have been linearized, but the Bose fields are site and time dependent. On the basis of the above formulae, one can easily study both magnetic ordering and the Kondo effect on the same footing by using a static saddle-point approximation.

2.3. Static saddle-point approximation

The simplest approximation to equations (10)–(12) is the static approximation, which is to neglect the time dependence of auxiliary Bose fields. For a FMKL system, we can also make a uniform approximation to neglect the site dependence of the fields. Within these approximations, the four auxiliary Bose fields are replaced by

$$x_i(\tau) = x \qquad \lambda_i(\tau) = E_0 \qquad m_{is}(\tau) = m_s \qquad m_{if}(\tau) = m_f. \qquad (13)$$

Here the parameters x, E_0, m_s and m_f are independent of imaginary time τ and site i, and their values are determined by a minimization of the free energy in the saddle-point approximation.

Substituting (13) into (12), one obtains a mean-field Hamiltonian of the renormalized hybridization band problem in k-space as

$$\begin{aligned} H_{MF} &= H_{eff}(x, E_0, m_s, m_f) \\ &= \sum_{k\sigma}\{(\epsilon_{k\sigma} c^{\dagger}_{k\sigma} c_{k\sigma} + E_{f\sigma} f^{\dagger}_{k\sigma} f_{k\sigma}) + Jx(f^{\dagger}_{k\sigma} c_{k\sigma} + c^{\dagger}_{k\sigma} f_{k\sigma})\} \\ &\quad -N(Jx^2 + \tfrac{1}{2} J m_s m_f + E_0) \end{aligned} \tag{14}$$

with

$$\epsilon_{k\sigma} = \epsilon_k - \tfrac{1}{2}\sigma J m_f \tag{15}$$

and

$$E_{f\sigma} = E_0 + \tfrac{1}{2}\sigma J m_s \tag{16}$$

representing the renormalized energies of conduction and f electrons, respectively. Now that H_{MF} (14) becomes quadratic in fermion operators, it can be diagonalized exactly. The quasi-particle energy obtained is of the form

$$\omega^{\pm}_{k\sigma} = \tfrac{1}{2}\{(\epsilon_{k\sigma} + E_{f\sigma}) \pm \sqrt{(\epsilon_{k\sigma} - E_{f\sigma})^2 + 4(Jx)^2}\}. \tag{17}$$

According to the Green function (GF) theory, the density of states (DOS) for the conduction electrons, denoted $\rho_{c\sigma}(\omega)$, and the DOS for the f electrons, denoted $\rho_{f\sigma}(\omega)$, in the MFA are

$$\rho_{c\sigma}(\omega) = \frac{1}{2D}[\theta(\omega - \epsilon_{a\sigma})\theta(\epsilon_{b\sigma} - \omega) + \theta(\omega - \epsilon_{c\sigma})\theta(\epsilon_{d\sigma} - \omega)] \tag{18}$$

$$\rho_{f\sigma}(\omega) = \frac{J^2 x^2}{2D(\omega - E_{f\sigma})^2}[\theta(\omega - \epsilon_{a\sigma})\theta(\epsilon_{b\sigma} - \omega) + \theta(\omega - \epsilon_{c\sigma})\theta(\epsilon_{d\sigma} - \omega)] \tag{19}$$

if the unperturbed DOS for conduction electrons takes the form

$$\rho^{(0)}_{c\sigma}(\omega) = \frac{1}{2D}\theta(\omega + D)\theta(D - \omega) \tag{20}$$

where $\theta(\omega)$ is the step function and D the half-width of the conduction band. The $\epsilon_{a\sigma}$, $\epsilon_{b\sigma}$, $\epsilon_{c\sigma}$ and $\epsilon_{d\sigma}$ are the edges of hybridized bands with spin σ, which are given by

$$\epsilon_{a\sigma} = \tfrac{1}{2}\{-D + E_{f\sigma} - \tfrac{1}{2} J m_f \sigma - \sqrt{[-D - E_{f\sigma} - \tfrac{1}{2} m_f \sigma]^2 + 4(Jx)^2}\} \tag{21a}$$

$$\epsilon_{b\sigma} = \tfrac{1}{2}\{D + E_{f\sigma} - \tfrac{1}{2} J m_f \sigma - \sqrt{[D - E_{f\sigma} - \tfrac{1}{2} m_f \sigma]^2 + 4(Jx)^2}\} \tag{21b}$$

$$\epsilon_{c\sigma} = \tfrac{1}{2}\{-D + E_{f\sigma} - \tfrac{1}{2} J m_f \sigma + \sqrt{[-D - E_{f\sigma} - \tfrac{1}{2} m_f \sigma]^2 + 4(Jx)^2}\} \tag{21c}$$

$$\epsilon_{d\sigma} = \tfrac{1}{2}\{D + E_{f\sigma} - \tfrac{1}{2} J m_f \sigma + \sqrt{[D - E_{f\sigma} - \tfrac{1}{2} m_f \sigma]^2 + 4(Jx)^2}\}. \tag{21d}$$

Now, we can calculate the free energy F in the static saddle-point approximation (MFA) directly from the partition function of a free-electron gas without using the functional integral representation for Z, the result is

$$\begin{aligned} F(m_f, m_s, x, E_0) &= -\beta^{-1} \sum_{k\sigma} (\ln\{1 + \exp[-\beta(\omega^{-}_{k\sigma} - \mu)]\} + \ln\{1 + \exp[-\beta(\omega^{+}_{k\sigma} - \mu)]\}) \\ &\quad -N(Jx^2 + \tfrac{1}{2} J m_s m_f + E_0). \end{aligned} \tag{22}$$

The values of the parameters m_f, m_s, x and E_0 can then be determined by the static saddle-point equations for FMKL through minimizing F with respect to those parameters:

$$m_f = \sum_\sigma \sigma \int_{-\infty}^{+\infty} f(\omega)\rho_{f\sigma}(\omega)\,\mathrm{d}\omega = \frac{1}{N}\sum_{k\sigma} \sigma \langle f_{k\sigma}^\dagger f_{k\sigma}\rangle_T \tag{23}$$

$$m_s = \sum_\sigma (-\sigma) \int_{-\infty}^{+\infty} f(\omega)\rho_{c\sigma}(\omega)\,\mathrm{d}\omega = \frac{1}{N}\sum_{k\sigma} (-\sigma)\langle c_{k\sigma}^\dagger c_{k\sigma}\rangle_T \tag{24}$$

$$x = \sum_\sigma \int_{-\infty}^{+\infty} \frac{Jxf(\omega)\rho_{c\sigma}(\omega)}{\omega - E_{f\sigma}}\,\mathrm{d}\omega = \frac{1}{N}\sum_{k\sigma}\langle f_{k\sigma}^\dagger c_{k\sigma}\rangle_T \tag{25}$$

$$1 = \sum_\sigma \int_{-\infty}^{+\infty} f(\omega)\rho_{f\sigma}(\omega)\,\mathrm{d}\omega = \frac{1}{N}\sum_{k\sigma}\langle f_{k\sigma}^\dagger f_{k\sigma}\rangle_T = n_f \tag{26}$$

where the GF method has been used. From equations (23)–(26), it is clear that m_s and m_f are the magnetizations of conduction and f electrons, respectively, representing the magnetic order parameters of the system; x is an order parameter describing the Kondo effect; E_0 is determined by the condition $n_f = \sum_\sigma \langle f_{i\sigma}^\dagger f_{i\sigma}\rangle_T = 1$, which shows that the constraint (3) is now satisfied in an average way. The chemical potential μ, which enters into the Fermi distribution function $f(\omega) = \{\exp[\beta(\omega-\mu)]+1\}^{-1}$, has to be obtained from the conservation of the total electron number $n_c + n_f$ per site. In cooperation with equation (26), we have an additional equation for fixing the chemical potential:

$$n_c = \sum_\sigma \int_{-\infty}^{+\infty} f(\omega)\rho_{c\sigma}(\omega)\,\mathrm{d}\omega. \tag{27}$$

Equations (23)–(27) constitute a set of fundamental mean-field equations, which will be used to determine the parameters m_s, m_f, x, E_0 and μ in a FMKL self-consistently.

3. Ground-state phase diagram

We now turn to construct the GSPD of the mean-field Hamiltonian (14) for arbitrary values of the exchange coupling $|J|/D$ and of the conduction band filling n_c. There are three types of phase that can arise in the ground state of H_{MF}. They are a pure Kondo phase, a pure ferromagnetic phase and the ferromagnetic–Kondo coexistent phase. The relative stabilities of these phases will be obtained by comparing their GSEs. The GSE of the FMKL per unit cell can be derived from H_{MF} at $T = 0$:

$$E_g = \sum_\sigma \int_{-\infty}^{\mu} \omega\rho_{c\sigma}(\omega)\,\mathrm{d}\omega - \tfrac{1}{2}n_c(n_c-2)D \tag{28}$$

where μ is the chemical potential at $T = 0$, i.e. the Fermi level. The origin of the GSE is taken to be the energy of the paramagnetic phase with $x = m_s = m_f = 0$. The results are as follows.

3.1. Pure Kondo phase

For the pure Kondo phase, we have $m_s = m_f = 0$. In this limiting case, the conduction electron DOS reverts to its unperturbed form equation (20), and equation (19) for the f DOS reduces to the simpler form

$$\rho_{f\sigma}(\omega) = \frac{J^2x^2}{2D(\omega - E_0)^2}[\theta(\omega-\epsilon_a)\theta(\epsilon_b-\omega) + \theta(\omega-\epsilon_c)\theta(\epsilon_d-\omega)] \tag{29}$$

with the band edges

$$\epsilon_a = \tfrac{1}{2}\{-D + E_0 - \sqrt{(D + E_0)^2 + 4(Jx)^2}\} \tag{30a}$$

$$\epsilon_b = \tfrac{1}{2}\{D + E_0 - \sqrt{(D - E_0)^2 + 4(Jx)^2}\} \tag{30b}$$

$$\epsilon_c = \tfrac{1}{2}\{-D + E_0 + \sqrt{(D + E_0)^2 + 4(Jx)^2}\} \tag{30c}$$

$$\epsilon_d = \tfrac{1}{2}\{D + E_0 + \sqrt{(D - E_0)^2 + 4(Jx)^2}\}. \tag{30d}$$

The order parameter x_K and GSE E_K can be easily obtained using the fundamental mean-field equations (23)–(27) and equation (28) as

$$\left(\frac{Jx_K}{D}\right)^2 = \frac{n_c \exp(-D/|J|)}{[1 - \exp(-D/|J|)]^2} \tag{31}$$

$$E_K = -\frac{n_c D \exp(-D/|J|)}{1 - \exp(-D/|J|)}. \tag{32}$$

3.2. Pure ferromagnetic phase

For the pure ferromagnetic phase with $m_f = 1$ and $x = 0$, we find that the hybridized f bands degenerate into f levels with an energy splitting of $|J|m_s$ between the spin-up and spin-down levels, and the f DOS becomes a delta function:

$$\rho_{f\sigma} = \delta(\omega - E_0 + \sigma|J|m_s/2). \tag{33}$$

At the same time, there is no hybridization gap in conduction bands, but only a band splitting of $|J|$ exists between different spin directions. Its conduction electron DOS can be written as

$$\rho_{c\sigma}(\omega) = (1/2D)\theta(\omega + D - \sigma|J|/2)\theta(D + \sigma|J|/2 - \omega). \tag{34}$$

The magnetization of the conduction electrons and the GSE are given by

$$m_s = \begin{cases} n_c & (n_c < |J|/2D) \\ |J|/2D & (n_c > |J|/2D) \end{cases} \tag{35}$$

and

$$E_{FM} = \begin{cases} -\frac{1}{2}n_c(|J|/D - n_c)D = E_{SFS} & (n_c < |J|/2D) \\ -|J|^2/8D = E_{RFS} & (n_c > |J|/2D). \end{cases} \tag{36}$$

We note that, for $n_c < |J|/2D$, only the spin-down band is occupied by the conduction electrons and the magnetization of conduction electrons approaches the saturation value $m_s = n_c$, which is called the saturated ferromagnetic state (SFS) [10]. Otherwise, in the case where $n_c > |J|/2D$, both spin-up and spin-down bands are occupied partially, and we then have the usual RFS.

3.3. Coexistent phase

We now discuss in detail the ferromagnetic–Kondo coexistent solutions with $x \neq 0$, $m_s \neq 0$ and $m_f \neq 0$. Generally speaking, for $0 < n_c < 1$ there are three cases corresponding to the different positions of Fermi level in hybridization bands.

(1) The Fermi level lies in lower hybridization bands for both spin projections.

(2) The Fermi level moves into the gap of spin-up bands but still lies in the lower spin-down band with increasing $|J|/D$ for fixed n_c.

(3) The Fermi level may enter the upper hybridization band for spin up and the lower band for spin down in the same region of $|J|/D$ as for case (2).

However, as shown in [11, 12], case (3) is believed to be energetically unfavourable for $0 < n_c < 1$. This has also been confirmed numerically by comparing its GSE with that of case (2). Therefore, we shall abandon case (3) and deal only with the coexistent solutions of the first two cases in the following discussion.

3.3.1. Case (1): $\epsilon_{a\sigma} < \mu < \epsilon_{b\sigma}$. Here, $\epsilon_{a\sigma}$ and $\epsilon_{b\sigma}$ are the edges of lower hybridization bands for spin σ given by equations (21*a*) and (21*b*). In this case the following exact formulae for the order parameters are derived:

$$m_f^2 = \frac{J_1 - n_c^2 J_2}{J_1 - \gamma^2 J_1} \tag{37a}$$

$$m_s^2 = \frac{J_1 - n_c^2 J_2}{1 - J_1 J_2} \tag{37b}$$

$$\left(\frac{J x_c}{D}\right)^2 = J_1 \frac{(1 + n_c J_2)^2 - (m_f + m_s J_2)^2}{(1 - J_1 J_2)^2} \tag{37c}$$

by solving $T = 0$ mean-field equations (23)–(27) self-consistently. The dimensionless parameters γ, J_1 and J_2 introduced in equation (37) are found to be

$$\gamma^2 = \frac{J_1}{1 - J_1 J_2 + J_2} = \gamma_{MRS}^2 \tag{38a}$$

$$J_1 = \left(\frac{|J|}{2D}\right)^2 - J_1 J_2 \left(1 + \frac{|J|}{2D}\right)^2 \tag{38b}$$

$$J_1 J_2 = \exp\left(-\frac{2D}{|J|}\right) \tag{38c}$$

which are independent of the concentration n_c in accordance with [10]. As a result, we find that with increase in $|J|/D$ the magnetization m_f for a fixed n_c is reduced by the enhancement of the Kondo effect, and the system enters into the pure Kondo state as shown in curve (1) of figure 1(a). So, we call it the moment-reduced state (MRS). The phase boundary between the MRS and the pure Kondo state can easily be obtained as

$$n_c = \sqrt{J_1/J_2} \tag{39}$$

by setting $m_s = m_f = 0$ in equation (37).

3.3.2. Case (2): $\epsilon_{a\downarrow} < \mu < \epsilon_{b\downarrow}$ *and* $\epsilon_{b\uparrow} < \mu < \epsilon_{c\downarrow}$. Since the Fermi level in this case lies in the gap region of spin-up electrons, i.e. the lower spin-up bands for both conduction and f electrons are fully occupied, the following relation can be established:

$$n_{c\uparrow} + n_{f\uparrow} = 1. \tag{40}$$

From the mean-field equations (23), (24) and (27), we also have the relation $m_f = n_{f\uparrow} - n_{f\downarrow}, m_s = n_{c\downarrow} - n_{c\uparrow}$ and $n_{f\uparrow} + n_{f\downarrow} = 1$. With these relations, we find that the total magnetization

$$m_t = m_f - m_s = 1 - n_c \tag{41}$$

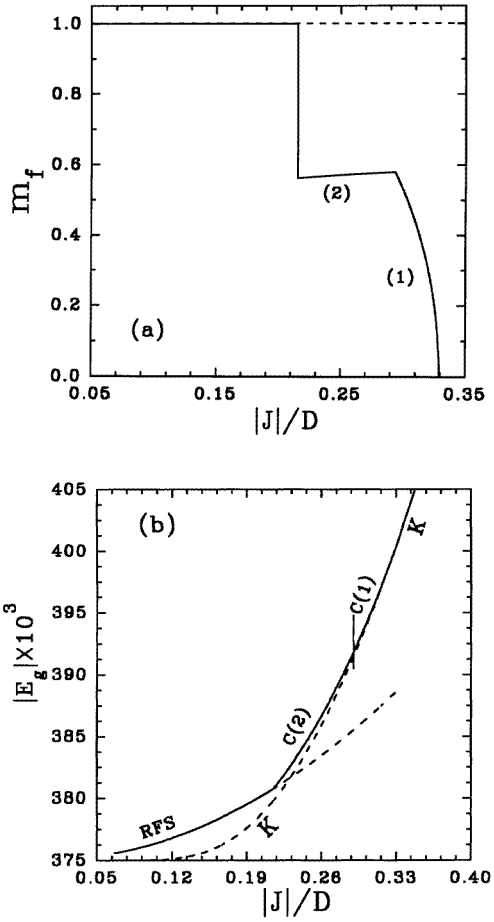

Figure 1. (a) The f-electron magnetizations m_f versus $|J|/D$ at $n_c = 0.5$, where curves 1 and 2 denote the two cases of ferromagnetic–Kondo coexistent states. (b) The absolute values of the GSEs $|E_g|$ for the pure Kondo state (curve K), the RFS (curve RFS) and the coexistent states of case 1 and 2 (curves C(1) and C(2)) vary with $|J|/D$ at $n_c = 0.5$. Here, the solid curves are the stable ground states, and the broken curves represent the energetically unfavourable states.

is independent of $|J|/D$ and takes the saturation value $1 - n_c$. On the other hand, if we set $m_f = \gamma m_s$ as in case (1), we can obtain the analytical expressions for m_f, m_s and x_c as

$$m_f = (1 - n_c)/(1 - \gamma) \tag{42a}$$

$$m_s = \gamma(1 - n_c)/(1 - \gamma) \tag{42b}$$

$$\left(\frac{Jx_c}{D}\right)^2 = J_1 \frac{(1 + n_c J_2)^2 - (m_f + m_s J_2)^2}{(1 - J_1 J_2)^2} \tag{42c}$$

where x_c satisfies the same form of expression as equation (37*c*), but the parameters γ, J_1 and J_2 must be determined by the following new relations:

$$\gamma = \frac{(|J|/2D)(1 - J_1 J_2) - J_1(1 + J_2)}{1 + J_2 - (|J|/2D)(1 - J_1 J_2)} = \gamma_{QSS} \tag{43a}$$

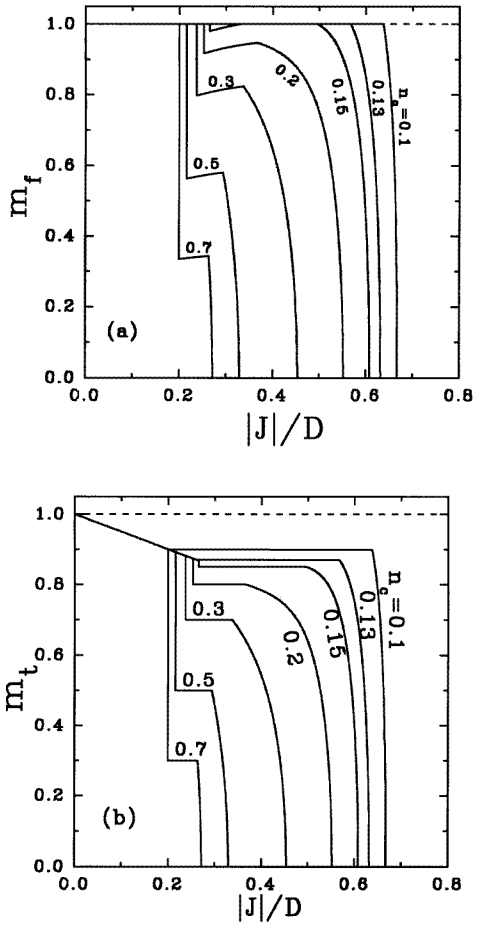

Figure 2. (a) The dependence of m_f on $|J|/D$ for various n_c. (b) The dependence of m_t on $|J|/D$ for various n_c.

$$\frac{J_1}{J_2} = 2\frac{n_c\gamma - 1}{n_c + \gamma - 2} - 1 \tag{43b}$$

$$J_1 J_2 = \exp\left(-\frac{2D}{|J|}\right). \tag{43c}$$

Obviously, the dimensionless parameters γ, J_1 and J_2 now become functions of both n_c and $|J|/D$, distinguishing themselves from case (1). The magnetization of f electrons as a function of $|J|/D$ for a fixed n_c has also been plotted in curve (2) of figure 1(a), where m_f is determined by equation (42*a*) and found to be approximately a linear function of $|J|/D$ which is different from the SFS with $m_f = 1$ and $m_s = n_c$. Meanwhile, the total magnetization m_t for a fixed n_c shows a plateau (see figure 2(b) below) and takes the saturation value $m_t = 1 - n_c$ similar to the SFS. Therefore, the coexistent solution shown in equation (42) behaves like quasi-saturation, and we can name it the quasi-saturated state (QSS).

The analytical expression of the GSE for the above two cases is obtained from equation (28) as

$$E_c = -\left[n_c\left(\frac{1+n_cJ_2}{1-J_1J_2}-1\right)+\frac{m_s^2}{2}\right]D+\frac{1}{2}m_s(E_{F\downarrow}-E_{F\uparrow}) \tag{44}$$

where $E_{F\uparrow}$ and $E_{F\downarrow}$ denote the energy levels which correspond to the upper occupation limits of spin-up and spin-down electrons, respectively. Here, we have $E_{F\uparrow}=E_{F\downarrow}=\mu$ for case (1) (MRS), but take $E_{F\uparrow}=\epsilon_{b\uparrow}$ and $E_{F\downarrow}=\mu$ in case (2) (QSS).

3.4. Ground-state phase diagram

So far, we have obtained the possible solutions of all cases for a FMKL. In order to get the stable GSPD, we should further compare their GSEs by using equations (32), (36) and (44). The GSEs of the pure Kondo state, the RFS and the ferromagnetic–Kondo coexistent state of cases (1) and (2) for $n_c=0.5$ are sketched in figure 1(b), where the solid curves represent the stable ground states after comparing their energies. We find that on decrease in $|J|/D$ the system changes gradually from the Kondo state with $m_f=0$ to the coexistent states (MRS and QSS) with $m_f<1$, and finally it jumps to the RFS with $m_f=1$ (see figure 1(a)), which means that there exists a first-order transition between the QSS and RFS.

The f-electron magnetization m_f and the total magnetization m_t versus $|J|/D$ for different values of the concentration n_c are given in figures 2(a) and 2(b), respectively. With these results and after comparing their GSEs, we obtain the $|J|/D$–n_c phase diagram at $T=0$ K as figure 3, that is the GSPD. The GSPD contains five states, i.e. the pure Kondo state, the MRS, the QSS, the SFS, and the usual RFS. The phase boundary between the Kondo and the MRS state is determined by equation (39), the boundary between the MRS and the QSS by $\gamma_{MRS}=\gamma_{QSS}$, the boundary between the QSS and the RFS by $E_{c(QSS)}=E_{RFS}$ and the boundaries between the SFS and the RFS, QSS and MRS are given by $n_c=|J|/2D$, $n_c=\gamma_{QSS}$ and $n_c=\gamma_{MRS}$, respectively. Furthermore, one can easily find from figure 3 that the changes in the ground state on increase in $|J|/D$ at a fixed n_c are as follows. For high concentrations ($n_c>0.15$), the ground state goes consecutively from RFS $\rightarrow$ QSS $\rightarrow$ MRS $\rightarrow$ Kondo state as mentioned above, while for the low concentrations ($n_c<0.15$), the SFS occurs instead of the QSS, and the ground state of the system then changes according to the following way: RFS $\rightarrow$ SFS $\rightarrow$ MRS $\rightarrow$ Kondo state. These indicate that the system evolves gradually into the Kondo phase with increasing $|J|/D$, which is one aspect of the competition between the Kondo and ferromagnetic phases. On the other hand, the results that the m_f–$|J|/D$ and m_t–$|J|/D$ curves move down with increase in n_c, as in figures 2(a) and 2(b), show us another aspect of the competitions due to the enhancement of Kondo screening as the concentration n_c of conduction electrons increases.

4. T_C–$|J|/D$ phase diagram

For a comprehensive understanding of the competition effects, in this section we shall extend our discussion on the phase diagram of a FMKL to finite temperatures. We shall first derive a formula which determines the Curie temperature T_C of the ferromagnetic–Kondo coexistent phase, and then the dependence of T_C on $|J|/D$ for different n_c is calculated by solving the $T>0$ mean-field equations (23)–(27) self-consistently.

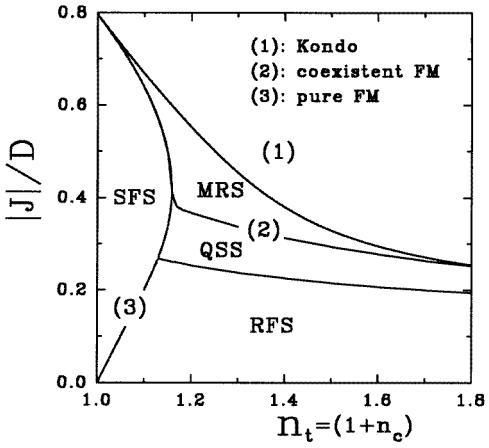

Figure 3. Zero-temperature phase diagram of the FMKL model: curve 1, Kondo phase; curve 2, coexistent ferromagnetic phase; curve 3, pure ferromagnetic phase.

4.1. T_C equation of the coexistent phase

The Curie temperature T_C here represents the transition temperature between the ferromagnetic–Kondo coexistent phase and the pure Kondo phase. It is determined by the conditions $m_f = m_s = 0$ and $x \neq 0$. In the region near T_C where m_f and m_s approach zero, one can expand the band edges shown in equation (21) only to first order in m_f and m_s. To this order of accuracy,

$$\epsilon_{a\sigma} = \epsilon_a + \sigma(|J|u_+/4)m_f + \sigma(|J|u_-/4)m_s \tag{45a}$$

$$\epsilon_{b\sigma} = \epsilon_b - \sigma(|J|v_-/4)m_f - \sigma(|J|v_+/4)m_s \tag{45b}$$

$$\epsilon_{c\sigma} = \epsilon_c - \sigma(|J|u_-/4)m_f - \sigma(|J|u_+/4)m_s \tag{45c}$$

$$\epsilon_{d\sigma} = \epsilon_d + \sigma(|J|v_+/4)m_f + \sigma(|J|v_-/4)m_s \tag{45d}$$

where

$$u_\pm = \frac{D + E_0}{\sqrt{(D + E_0)^2 + 4(Jx)^2}} \pm 1 \tag{46a}$$

$$v_\pm = \frac{D - E_0}{\sqrt{(D - E_0)^2 + 4(Jx)^2}} \pm 1. \tag{46b}$$

Here ϵ_a, ϵ_b, ϵ_c and ϵ_d are the band edges of the Kondo phase which have been given in equation (30). Substituting equations (45) and (46) into the mean-field equations (23) and (24), we obtain the following linear equations of m_f and m_s for temperatures just below T_C:

$$m_f = \alpha m_f + \beta m_s \tag{47a}$$

$$m_s = \xi m_f + \eta m_s. \tag{47b}$$

The T_C equation of the ferromagnetic–Kondo coexistent phase is then found to be

$$(1 - \alpha)(1 - \eta) = \beta\xi \tag{48}$$

with

$$\alpha = \frac{J^2x^2}{2D}\left(\frac{f(\epsilon_d)}{(\epsilon_d - E_0)^2}v_+ + \frac{f(\epsilon_c)}{(\epsilon_c - E_0)^2}u_- - \frac{f(\epsilon_b)}{(\epsilon_b - E_0)^2}v_- - \frac{f(\epsilon_a)}{(\epsilon_a - E_0)^2}u_+\right) \tag{49a}$$

$$\beta = \frac{J^2x^2}{2D}\left(\frac{f(\epsilon_d)}{(\epsilon_d - E_0)^2}v_- + \frac{f(\epsilon_c)}{(\epsilon_c - E_0)^2}u_+ - \frac{f(\epsilon_b)}{(\epsilon_b - E_0)^2}v_+ - \frac{f(\epsilon_a)}{(\epsilon_a - E_0)^2}u_-\right) - 2|J|\left(\int_{\epsilon_a}^{\epsilon_b} + \int_{\epsilon_c}^{\epsilon_d}\right)\frac{f(\omega)}{(\omega - E_0)^3}\,\mathrm{d}\omega \tag{49b}$$

$$\xi = \frac{1}{2D}[f(\epsilon_a)u_+ + f(\epsilon_b)v_- - f(\epsilon_c)u_- - f(\epsilon_d)v_+] \tag{49c}$$

$$\eta = \frac{1}{2D}[f(\epsilon_a)u_- + f(\epsilon_b)v_+ - f(\epsilon_c)u_+ - f(\epsilon_d)v_-] \tag{49d}$$

where $f(\omega)$, $f(\epsilon_a), \ldots$ and $f(\epsilon_d)$ are the Fermi distributions at $T = T_C$.

To find the dependence of T_C on $|J|/D$ at a fixed n_c, we have to perform numerical calculations of equations (48) and (49), in which the quantities x, E_0 and μ must be obtained self-consistently from the following mean-field equations at $T = T_C$:

$$n_f = \frac{J^2x^2}{D}\left(\int_{\epsilon_a}^{\epsilon_b} + \int_{\epsilon_c}^{\epsilon_d}\right)\frac{f(\omega)}{(\omega - E_0)^2}\,\mathrm{d}\omega = 1 \tag{50a}$$

$$n_c = \frac{1}{D}\left(\int_{\epsilon_a}^{\epsilon_b} + \int_{\epsilon_c}^{\epsilon_d}\right)f(\omega)\,\mathrm{d}\omega \tag{50b}$$

$$x = -\frac{|J|x}{D}\left(\int_{\epsilon_a}^{\epsilon_b} + \int_{\epsilon_c}^{\epsilon_d}\right)\frac{f(\omega)}{\omega - E_0}\,\mathrm{d}\omega. \tag{50c}$$

In a similar way, the transition temperature T_{RKKY} of the pure ferromagnetic phase can also be derived from the mean-field equations with the use of equations (33) and (34) as the f DOS and conduction electron DOS, respectively. The result takes the usual form

$$k_BT_{RKKY} = |J|^2/8D = |E_{RFS}| \tag{51}$$

which is equal to the absolute value of GSE in the RFS. In order to clarify the competition between ferromagnetic order and the Kondo effect in the coexistent phase, we still have to introduce the Kondo temperature T_K. As an energy scale, k_BT_K is usually defined by the difference between the GSEs of the pure Kondo phase and the paramagnetic phase with $x = 0$ [15]. Thus we have

$$k_BT_K = n_cD\exp(-D/|J|)/[1 - \exp(-D/|J|)] = |E_K| \tag{52}$$

which is just the absolute value of E_K in equation (32).

4.2. T_C–$|J|/D$ phase diagram for different n_c

Our theoretical T_C–$|J|/D$ curve for a fixed concentration $n_c = 0.2$ is shown in figure 4(a), where T_{RKKY} and T_K are also sketched. It is clear that figure 4(a) contains the basic information of Doniach's bell-shaped phase diagram. In the weak-coupling region where $T_{RKKY} \gg T_K$, the variation in T_C with $|J|/D$ coincides with that of T_{RKKY} which is proportional to J^2, and the system stays in the RKKY ferromagnetic phase. In the intermediate-coupling region where T_K increases rapidly with increasing $|J|/D$, it approaches and even goes beyond the value of T_{RKKY}. In this case the competition between the Kondo effect and ferromagnetic order comes into force, which makes the system change from the RKKY ferromagnetic phase to the coexistent phase. As a result, the increment of T_C with increasing $|J|/D$ is lowered and T_C arrives at a maximum when $T_K \simeq T_{RKKY}$, which reflects the behaviour of

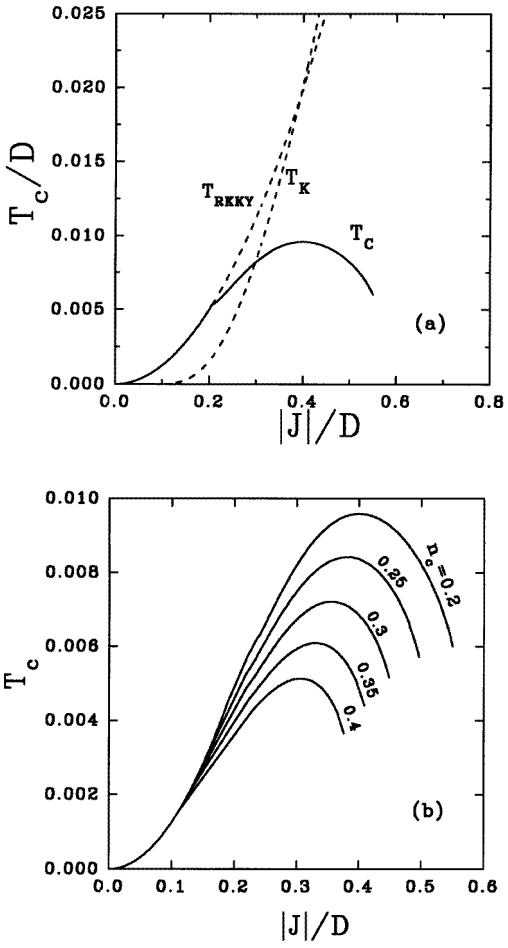

Figure 4. (a) The Curie temperature T_C of the ferromagnetic–Kondo coexistent phase versus $|J|/D$ at $n_c = 0.2$, where T_{RKKY} is the Curie temperature of the RKKY ferromagnetic phase and T_K is the Kondo temperature. (b) The T_C–$|J|/D$ curves for various values of n_c.

the QSS. With further increasing coupling, T_C becomes a decreasing function of $|J|/D$ when $T_K > T_{RKKY}$, where the coexistent MRS comes into being because of suppression of ferromagnetic order by the Kondo effect as mentioned above in section 3. In the strong-coupling region where $T_K \gg T_{RKKY}$, T_C drops rapidly, and finally the system moves into the non-magnetic Kondo phase. Therefore, the schematically bell-shaped phase diagram proposed by Doniach [7] is reproduced from a 3D FMKL model using the functional integral method.

The numerical results of the T_C–$|J|/D$ curves for different concentrations n_c have also been obtained and are shown in figure 4(b), which can give us further information about the phase diagram in the T_C–$|J|$ plane. Note that the T_C–$|J|/D$ curve in the intermediate-coupling region moves downwards increasingly with increasing n_c. Physically, the enhancement of the Kondo screening with increase in the conduction electron concentrations is responsible for this interesting result. The corresponding result at $T = 0$ has already been obtained in figure 2(b), where the m_t–$|J|/D$ curve also shown a downturn behaviour as n_c increases, for the same reason. Both the results are of use for the HF ferromagnets.

5. Conclusions and discussion

Now we conclude this paper with some discussion, attempting to compare our theoretical results with the experiments on HF ferromagnets. We have presented a SCMF theory to investigate the phase diagram of a FMKL model by adopting the functional integral formalism with four auxiliary Bose fields. In this formalism both the Kondo effect and ferromagnetic order can be studied on the same footing. The ferromagnetic–paramagnetic (Kondo) phase diagrams including the ferromagnetic–Kondo coexistent phase at $T = 0$ and $T > 0$ have been obtained. The main results which are useful for qualitatively explaining the experiments are as follows.

(1) For a fixed concentration n_c, the dependence of the Curie temperature T_C on the exchange-coupling strength $|J|/D$ given in figure 4(a) behaves according to the bell-shaped phase diagram proposed by Doniach [7], which is thought to be a universal phase diagram of the HF magnets [5].

(2) As shown in figure 4(b), the bell-shaped T_C–$|J|/D$ curve shifts downwards with increasing conduction electron concentration n_c.

(3) The total magnetization m_t versus $|J|/D$ also shows a consecutive downturn with increase in n_c, as sketched in figure 2(b).

All in all, the magnetic properties of a FMKL system are determined by both $|J|/D$ and n_c, which are controlled experimentally by chemical substitution and the application of pressure. The application of pressure is known to increase the value of $|J|/D$ in Ce compounds [16]. However, there are at least two cases for chemical substitution in HF ferromagnets, e.g. in the ternary Ce compound $CeRh_3B_2$. The first case is the change in $|J|/D$ at a fixed value of n_c in the $CeRh_3(B_{1-y}Si_y)_2$ series by substituting Si for B to expand the lattice, and the expansion of the lattice would be expected to decrease the magnitude of $|J|/D$ [5, 17]. Note that the coupling $|J|$ in $CeRh_3B_2$ is proportional to $|V|^2_{df}$, where V_{df} is the strength of f–d hybridization between the f electrons of Ce and the conduction electrons from the 4d band of Rh [17]. Obviously, Si substitution does not change the conduction electron concentration n_c of the 4d electrons in Rh, and the only change is the suppression of $|J|/D$ due to the cell-volume expansion by doping with Si in $CeRh_3B_2$ [5]. The second case is concerned with the substitution of Ru for Rh in the $Ce(Rh_{1-y}Ru_y)_3B_2$ series, where the increase in the concentration n_c of the 4d conduction electrons has been observed directly by XPS measurements, but the cell volume remains unchanged upon doping of Ru [5, 18]. Thus we have the case of increasing n_c with a fixed value of $|J|/D$ in the Ru substitution system.

We now compare our theoretical results with the experiments on $CeRh_3B_2$ as follows.

(1) As pointed out by Cornelius and Schilling [5], the results for both pressure measurements on $CeRh_3B_2$ and Si substitution experiments are in good agreement with each other. Both data roughly follow a bell-shaped T_C–$|J|/D$ curve which resembles the schematic phase diagram presented by Doniach. It is seen to be in reasonably good agreement with our theoretical curve of T_C–$|J|/D$ for a fixed value of n_c.

(2) For Ru substitution in the $Ce(Rh_{1-y}Ru_y)_3B_2$ series, one can find that T_C drops vertically at a fixed value of $|J|$ with increasing doping concentration y from the data collected in [5]. We caution that this can be considered as the second case of chemical substitution mentioned above. In this case the Curie temperature T_C of the system has to go downwards along the vertical line with a fixed $|J|$ owing to the enhancement of Kondo screening as n_c increases. Therefore, the results for $Ce(Rh_{1-y}Ru_y)_3B_2$, which had been considered as an exception to Doniach's phase diagram in [5], can now be explained by

the theoretical results given in figure 4(b). In fact, it is an extension of Doniach's phase diagram (i.e. the T_C–$|J|/D$ curve) to cases with variable n_c.

(3) The saturation moment of the $Ce(Rh_{1-y}Ru_y)_3B_2$ system shows a similar downward behaviour with increasing n_c [5], which is also in qualitative agreement with the results shown in figure 2(b), where the m_t–$|J|/D$ curve shifts downwards as the concentration n_c increases. The results of both (2) and (3) can be explained by the competition between the Kondo effect and ferromagnetic order, which have been given in sections 3.4 and 4.2.

It is perhaps interesting to compare our results with the previous theoretical works [8, 9]. Because of neglect of the competition between the pure Kondo and the pure ferromagnetic states, it was impossible to obtain the ferromagnetic–Kondo coexistent solutions in [8, 9]. After taking this point into account, we obtained a rather complete phase diagram. Apart from the pure Kondo state and pure RFS, it also includes the coexistent states, namely the MRS and the QSS, which play important roles in the finite-temperature properties of the system.

Finally, we would like to mention that, although the above discussion is valid only in the framework of the SCMF approximation, we have succeeded in reproducing the schematic phase diagram proposed by Doniach and also in obtaining its extended version for the cases with variable n_c from a 3D FMKL model. These are of practical use for qualitatively explaining the experimental observations in HF magnets.

Acknowledgment

This work was supported in part by the National Natural Science Foundation of China.

References

[1] Grewe N and Steglich F 1991 *Handbook on the Physics and Chemistry of Rare Earths* ed K A Gschneidner Jr and L Eyring (New York: Elsevier) ch 97, p 343
[2] Yashima H, Sato N, Mori H and Satoh T 1982 *Solid State Commun.* **43** 595
[3] Gignoux D and Gomez-Sal J C 1984 *Phys. Rev.* B **30** 3967
[4] Malik S K and Adroja D T 1991 *Phys. Rev.* B **43** 6295
[5] Cornelius A L and Schilling J S 1994 *Phys. Rev.* B **49** 3955
[6] Doniach S 1977 *Physica* B **92** 231
[7] Doniach S 1977 *Valence Instability and Related Narrow Band Phenomena* ed R D Parks (New York: Plenum) p 169
[8] Lacroix C and Cyrot M 1979 *Phys. Rev.* B **20** 1969; 1980 *J. Magn. Magn. Mater.* **15–18** 65
[9] Fazekas P and Müller-Hartmann 1991 *Z. Phys.* B **85** 285
[10] Li Z Z and Qiu Y 1985 *Chinese Phys. Lett.* **2** 553
[11] Zhuang M, Xiao M W and Li Z Z 1995 *Solid State Commun.* **94** 771
[12] Irkhin V Yu and Katsunelson M I 1991 *Z. Phys.* B **82** 77
[13] Coleman P and Andrei N 1989 *J. Phys.: Condens. Matter* **1** 4057
[14] Lacroix C 1991 *J. Magn. Magn. Mater.* **63–4** 90
[15] Read N and Newns D M 1983 *J. Phys. C: Solid State Phys.* **16** 3273; 1984 *Solid State Commun.* **52** 993
[16] Schilling J S 1979 *Adv. Phys.* **28** 657
[17] Malik S K, Shenoy G K, Dhar S K, Paulose P L and Vijayaraghavan R 1986 *Phys. Rev.* B **34** 8196
[18] Allen J W, Maple M B, Kang J S, Yang K N, Torikachvili M S, Lassailly Y, Eillis W P, Pate B B and Lindau I 1990 *Phys. Rev.* B **41** 9013